PAPER

Check for updates

The effects of calcination atmosphere on the catalytic performance of Ce-doped TiO$_2$ catalysts for selective catalytic reduction of NO with NH$_3$†

Yiqing Zeng,[a] Shule Zhang, [ID] *[a] Yanan Wang,[a] Guangli Liu[b] and Qin Zhong*[a]

A series of well-reported Ce$_x$–Ti catalysts with a low content of Ce species were synthesized by a sol–gel method. The aim of this study was to investigate the influence of different calcination atmospheres on the formation of the Ce–O–Ti structure that comprises active sites for the selective catalytic reduction (SCR) of NO by NH$_3$. Catalytic activity tests showed that the Ce$_x$–Ti–N (calcined under a nitrogen atmosphere) catalysts exhibited a significantly higher NO removal efficiency than Ce$_x$–Ti–A (calcined under air). Characterization results confirmed that more Ce species could incorporate into the TiO$_2$ lattice when calcined under a nitrogen atmosphere, thus, more Ce–O–Ti structures were obtained over the Ce$_x$–Ti–N surface. This improved the NH$_3$ adsorption and electron transfer from Ti to Ce. Therefore, N$_2$ calcination increased the acid sites and improved the redox ability for Ce$_x$–Ti–N catalysts. In addition, it was found that the redox ability was the critical factor, which effectively promoted the low temperature SCR performance. Amongst the Ce$_x$–Ti–N catalysts, Ce$_5$–Ti–N revealed the best SCR activity, catalytic stability and resistance to H$_2$O and SO$_2$. This study demonstrated the feasibility of N$_2$ calcination in the syntheses of doped SCR catalysts and also explored the SCR reaction mechanism over the well-reported Ce$_x$–Ti catalysts. We expect that this study could shed some light on the development of feasible preparative routes for the syntheses of Metal-Ti catalysts for SCR application.

1. Introduction

NO$_x$ emitted from coal-fired power plants remains a major source of photochemical smog, acid rain and the depletion of tropospheric ozone.[1] At present, the selective catalytic reduction (SCR) of NO$_x$ with NH$_3$ in the presence of excess oxygen on commercial V$_2$O$_5$/WO$_3$ (MoO$_3$)/TiO$_2$ is the most widely used technology for the removal of NO$_x$.[2] However, some critical problems, such as a high temperature window (>320 °C) and the toxicity of vanadium species, still exist in the practical applications of vanadium-based catalysts. Considering these disadvantages, many researchers focus on studies to replace the vanadium with other metal elements.[3] CeO$_2$–TiO$_2$ based catalysts are considered a potential replacement of V$_2$O$_5$/WO$_3$–TiO$_2$ catalysts due to their excellent NO conversion, high N$_2$ selectivity in SCR and environmentally friendly features.[4–7]

The SCR mechanism of CeO$_2$–TiO$_2$ based catalysts had been widely study, and the excellent performance of cerium oxide catalysts could be attributed to their high oxygen storage capacity, strong interaction with metals, good redox properties (redox couple of Ce^{3+}/Ce^{4+}).[8–10] For Ce-doped TiO$_2$ catalysts, the Ce–O–Ti short-range order species with the interaction between Ce and Ti in atomic scale are considered to be the active sites.[11–16] To obtain better catalytic activity, many methods that could strengthen the interaction between Ce and Ti in atomic scale have been used to modifying the Ce-doped TiO$_2$ catalysts.[16–18] Shan *et al.* has reported that Fe, Mo and W doping, especially W, could effectively improve the NO removal efficiency of Ce-doped TiO$_2$ catalysts, because the introduction of W species could increase the amount of active sites, oxygen vacancies, and Brønsted and Lewis acid sites over the catalyst.[17] According to the studies of Liu *et al.*, the preparative routes of catalysts has significantly effects on its physical/chemical properties, and a strong metal-support interaction for Ce-doped TiO$_2$ catalysts could obtained by using a supercritical water synthesis route.[16] Although numerous works having been conducted to strengthen the interaction between Ce and Ti, studies on calcination atmospheres seemed being given very little care. As a matter of fact, the physical/chemical properties of the catalysts are strongly relied on the calcination atmospheres. Thus, researches on the effects of calcination atmospheres on Ce-doped TiO$_2$ catalysts would be very necessary.

Herein, a series of Ce-doped TiO$_2$ catalysts calcined under air or nitrogen atmosphere were prepared by sol–gel method. Catalytic performance test proposed that the Ce-doped TiO$_2$

[a]School of Chemical Engineering, Nanjing University of Science and Technology, Nanjing 210094, PR China. E-mail: shulezhang@163.com; Fax: +86 25 84315517; Tel: +86 25 84315517

[b]Lanzhou Petrochemical Research Center, PetroChina, Lanzhou 730060, PR China

catalysts calcined in nitrogen atmosphere displayed a higher NO removal efficiency than that calcined under air. To elucidate the effect of calcination atmosphere, XRD, BET, NH_3-TPD, H_2-TPR, XPS and *in situ* DRIFT were used to study the structure, surface acidity, redox properties and surface composition of samples. It was found that more Ce species could dope into the TiO_2 lattice when calcined under nitrogen atmosphere, thus, more Ce–O–Ti structure were obtained over the Ce_x–Ti–N surface. This effect could improve the surface area, surface acidity and redox ability. In addition, we made clear the relationship the surface area, surface acidity and redox ability for the SCR activity and found that redox ability was the critical factor, which effectively promoted its SCR performance at low temperature. This information would contribute to a better way to prepare the Ce–Ti catalyst and a better understanding of the SCR processes over Ce system SCR catalysts.

2. Experimental

2.1 Catalysts preparation

The catalysts were prepared by a sol–gel method. A certain nitrate hexahydrate was dissolved into 80 mL ethanol, then 20 mL tetrabutyl titanate were dropped into under vigorous stirring, and then stirring at room temperature for 30 min to obtain solution A. Subsequently, a mixed solution of 20 mL ethanol, 8 mL deionized water and 8 mL acetic acid were dropped into solution A. After stirring at room temperature for 2 h, the solution heat in a water bath at 60 °C to obtain transparent sol. The transparent sol kept at room temperature overnight. Then the gel was dried at 120 °C to form xerogel, and half them calcined at 500 °C in air and N_2 atmosphere for 3 h, respectively. Finally, Ce_x–Ti–A (calcined under air atmosphere, x represent the CeO_2 contents in weight) and Ce_x–Ti–N (calcined under N_2 atmosphere) samples were obtained.

2.2 Catalytic activity tests

The SCR of NO_x was carried out at 120–300 °C in a fixed-bed flow reactor (i.d. 6.8 mm) using 0.2 mL catalyst with 100–120 mesh under atmospheric pressure. The typical reactant gas composition was as follows: 500 ppm NO, 500 ppm NH_3, 5% O_2 and N_2 as the balance gas. Total flow rate was 150 mL min^{-1}, corresponding to a space velocity of about 45 000 h^{-1}. The concentration of NO_x, N_2O in the inlet and outlet gas was measured by *in situ* FT-IR gas analyzer SERVOPRO 4900. The values of NO conversion can be calculated by:

$$NO \text{ conversion } (\%) = ([NO]_{in} - [NO_x]_{out})/NO_{in} \times 100\%$$

where NO_x = NO + NO_2.

2.3 Characterization

The crystal phase composition of samples was determined by X-ray diffraction measurements (Purkinje General Instrument Cu, Ltd, China, XD-3) at room temperature. The Brunauer–Emmett–Teller (BET) surface areas of the products were determined using a nitrogen adsorption analyzer (Quadrasorb-S1, Quantachrome,

USA) and the pore-size distribution was estimated by the Barrett–Joyner–Halenda method. X-ray photoelectron spectroscopy (XPS) was carried out on a RBD upgraded PHI-5000C ESCA system (Perkin Elmer) with Mg Kα radiation ($h\nu$ = 1253.6 eV), calibrated by the C 1s peak at 284.6 eV with an accuracy of $\pm$ 0.2 eV.

Ammonia temperature-programmed desorption (NH_3-TPD) and hydrogen temperature-programmed reduction (H_2-TPR) experiments were carried out in quartz U-tube reactor on an automated chemisorption analyzer (Quantachrome Instruments). Each catalyst was preheated at 120 °C for 24 h before TDP and H_2-TPR experimental and about 100 mg of sample was used. The TDP experimental began with NH_3 adsorption under a flow rate of 60 mL min^{-1} at room temperature for 1 h. Then the gas was switch to He for 0.5 h. Subsequently, TPD was performed by ramping the temperature at 10 °C min^{-1} to 800 °C in He (60 mL min^{-1}). In the H_2-TPR experimental, the sample was purged with 60 mL min^{-1} He at 50 °C for 0.5 h and then heating the sample to 800 °C at a rate of 10 °C min^{-1} after switched to a H_2/N_2 gas mixture (10% H_2, v/v) at a flow rate of 60 mL min^{-1}. The consumption of H_2, NH_3 was detected by a thermal conductivity detector (TCD).

In situ FTIR experiments were carried out by a Nicolet IZ10 FTIR spectrometer, equipped with a liquid-nitrogen cooled MCT detector. Prior to each experiment, background was taken by recording the IR spectrum of KBr in a N_2 stream at 300 °C, and had been deducted for each spectrum. During the experiment, 32 scans were averaged for each IR spectra, which were recorded at a resolution of 4 cm^{-1}. The reaction conditions were as follows: 500 ppm NO, 500 ppm NH_3, 5% O_2, N_2 as the balance gas and a 35 mL min^{-1} flow rate. Each catalyst was preheated at 300 °C for 60 min in N_2, and then cooled to 240 °C in 10 °C min^{-1}. After 30 min, the spectra were recorded as initial spectra. Then the $NH_3/(NO + O_2)$ were introduced to the gas chamber and the spectra were recorded at the desired time.

3. Result and discussion

3.1 SCR catalytic activity

NH_3-SCR performances of Ce–Ti–N and Ce–Ti–A catalysts with 2–10% CeO_2 were measured as a function of temperature, and the results are shown in Fig. 1. It was obvious that the SCR activity of Ce_x–Ti–A and Ce_x–Ti–N increased with the increase of
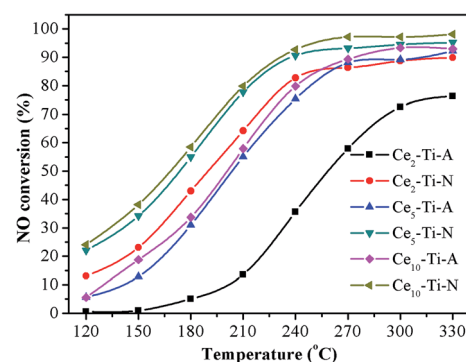

Fig. 1 NO conversion of Ce_x–Ti–A and Ce_x–Ti–N catalysts.

Ce content. Additionally, the NO conversion of Ce$_x$–Ti–N catalysts was much more prominent than that of Ce$_x$–Ti–A. The NO conversion of Ce$_5$–Ti–N catalyst was 54.9%, 77.8% and 90.7% at 180, 210 and 240 °C, respectively, and it increased by 24.0%, 22.8% and 15.4% compared with Ce$_5$–Ti–A at the same reaction temperatures. Interestingly, the NO removal efficiency over Ce$_2$–Ti–N was even higher than Ce$_{10}$–Ti–A when the reaction temperature below 240 °C, indicating that content of CeO$_2$ was not the critical factor in determining the catalytic activity of Ce–Ti. According to the previous studies, the Ce–O–Ti short range structure is the active sites for Ce–Ti catalyst in the SCR reaction.[11,12,19,20] Hence, more Ce–O–Ti structures might exist in Ce$_2$–Ti–N in comparison with Ce$_{10}$–Ti–A catalyst. This would be discussed in next sections. The remarkable point was that only a slight amount of N$_2$O (<5 ppm) appeared over all of the catalysts during experiments, indicating that all the prepared catalysts showed a good N$_2$ selectively.

3.2 The durability and stability

Ce$_5$–Ti–N was chosen as representative for investigating the catalytic stability of Ce$_x$–Ti–N catalysts. Fig. 2 shows the durability test results of Ce$_5$–Ti–N. It was clear that no deactivation occurred during 70 h at 240 °C. After that, four SCR reaction cycles at 120–240 °C was carried out. As shown in illustration, the NO conversion was almost same at each cycle. Therefore, the active sites of Ce$_5$–Ti–N catalyst were stable. The resistance to H$_2$O, SO$_2$ at 250 °C was also tested (Fig. S1†). The catalytic activity of Ce$_5$–Ti–N showed a slightly increase after 5% of H$_2$O was introduced. However, the lowest NO conversion with 5% of H$_2$O and 500 ppm SO$_2$ was 68.33%. It was worth noting that as the H$_2$O and SO$_2$ cut off, the catalytic activity of Ce$_5$–Ti–N could recover by raising reaction temperature to 300 °C. Then, as the reaction temperature was reduced back to 250 °C, the NO conversion restored to the initial state and kept stable. The results clearly suggested that the deposit of ammonium sulphate was the main cause for the loss of SCR activity as SO$_2$ was introduced. Therefore, the Ce$_5$–Ti–N catalysts displayed a good resistance to H$_2$O and SO$_2$.

3.3 XRD characterization

The XRD patterns of prepared catalysts are showed in Fig. 3. For all the catalysts, only anatase phase (2θ = 25.5°, 37.1°, 48.3°,
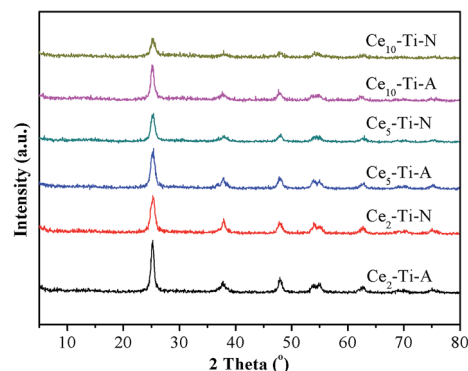

Fig. 2 The durability test result of Ce$_5$–Ti–N.

Fig. 3 XRD results of Ce$_x$–Ti–A and Ce$_x$–Ti–N catalysts.

54.1°, 55.3°, 62.8°, 70.3°, 75.3°) (PDF#21–1272) was observed, indicating that Ce species dispersed well. It can also be seen that the intensity of the peaks due to anatase TiO$_2$ decreased with the accumulation of Ce content. This result means that the interaction between Ce and Ti in atomic scale had a significantly enhancement by increasing the Ce content.[4] The previous studies had confirmed that the Ce–Ti catalyst had a higher NO conversion than the supported CeO$_2$/TiO$_2$ catalysts, and the interaction between Ce and Ti in atomic scale was via a Ce–O–Ti short-range order species in Ce-doped TiO$_2$ catalysts, which would significantly improve the NH$_3$-SCR performance.[11] Hence, with the increase of Ce content, the higher NH$_3$-SCR performance could be attributed to the accumulation of Ce–O–Ti short-range order species in catalysts. As compared to Ce$_x$–Ti–A catalysts, weaker diffraction peaks due to anatase TiO$_2$ could be observed on Ce$_x$–Ti–N catalysts. These results meant that the N$_2$ calcination atmosphere could promote the incorporation of Ce species into TiO$_2$ lattice. More Ce–O–Ti structure could form in Ce$_x$–Ti–N catalysts, which could significantly improve it's the catalytic activity.

3.4 BET results

The BET results of prepared catalysts are summarized in Table 1. In compared with Ce$_5$–Ti catalysts, Ce$_2$–Ti and Ce$_{10}$–Ti catalysts exhibited a much lower surface area. It indicated that suitable content of Ce doping could effectively improve the specific surface areas of the catalysts, because suitable Ce content could inhibit the agglomeration of the TiO$_2$ crystallites. These results well agreement to the results of previous
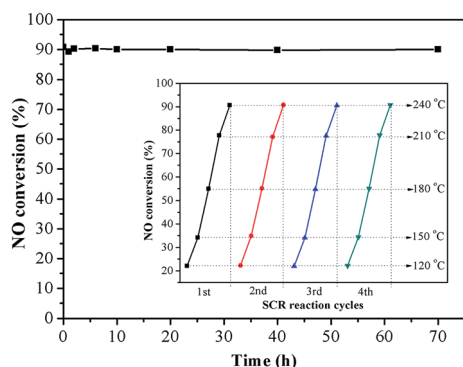
Table 1 BET data of Ce$_x$–Ti–A and Ce$_x$–Ti–N$_2$ catalysts

Sample	Surface area (m^2 g^{-1})	Pore volume (cm^3 g^{-1})	Pore size (nm)
Ce$_2$–Ti–A	51.1	0.061	5.610
Ce$_2$–Ti–N	109.2	0.097	5.597
Ce$_5$–Ti–A	152.7	0.308	9.519
Ce$_5$–Ti–N	178.0	0.335	9.529
Ce$_{10}$–Ti–A	106.3	0.127	4.883
Ce$_{10}$–Ti–N	86.2	0.105	4.893

studies.[4,11,17] It was clear that the Ce_5–Ti–A had a higher surface area than the Ce_2–Ti–N catalyst, but it showed a much lower SCR activity. Therefore, the surface area was not the critical factor to the catalytic activity difference of Ce_x–Ti–A and Ce_x–Ti–N catalysts.

3.5 Raman analysis

To further investigate the role of the N_2 calcination atmosphere in formation of short order Ce–O–Ti species, the catalysts were characterized by Raman. As shown in Fig. 4, all the catalysts only showed Raman-active modes of the anatase phase, indicating that a high dispersion or an incorporation of Ce species into the TiO_2 support for the catalysts.[21,22] This was well consistent with the result of XRD. As compared to Ce_x–Ti–A, a slight shift of E_g (TiO_2) peak was observed in Ce_x–Ti–N catalysts, indicating that the interaction between Ce species and TiO_2 supports in Ce_x–Ti–N was stronger than that over Ce_x–Ti–A catalyst. More importantly, the intensity of Raman peak of Ce_x–Ti–N catalysts decreased significantly compared with Ce_x–Ti–A catalysts. In general, the larger of the content of symmetric vibration bonds, the stronger the Raman signal. Therefore, the reduction of Raman signals could be attributed to the decrease of the amount of Ti–O–Ti symmetric vibration, which was resulted from more Ce–O–Ti formation. It suggested that more CeO_2 was on Ce_x–Ti–A catalysts than that of Ce_x–Ti–N and N_2 calcination improved Ce species into TiO_2 to form more Ce–O–Ti structure. The decrease of Raman peak of catalysts with lower Ce content in this study was similar to SC-$Ce_{0.25}TiO_2$ (25 wt%) and AM-CeTi (30 mol%) catalysts of previous studies.[13,16]

3.6 XPS analysis

The incorporation of Ce ions into TiO_2 lattice would lead to the changes of chemical surrounding of surface species.[23,24] To investigate the effects of N_2 calcination atmospheres on surface component and chemical state of elements in catalysts, XPS was used. Fig. 5a displays the XPS results of Ti 2p. As compared to P25 (Degussa), the peaks of Ce_5–Ti–A catalysts shifted to a high binding energy, indicating that the Ti species of Ce–Ti–A had a lower density of electron cloud than that of TiO_2. This result could be attributed to the formation of Ce–O–Ti due to the larger electronegativity of Ce^{4+} than Ti^{4+}. In comparison to Ce_5–
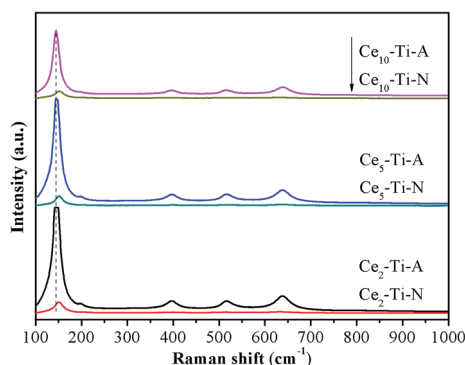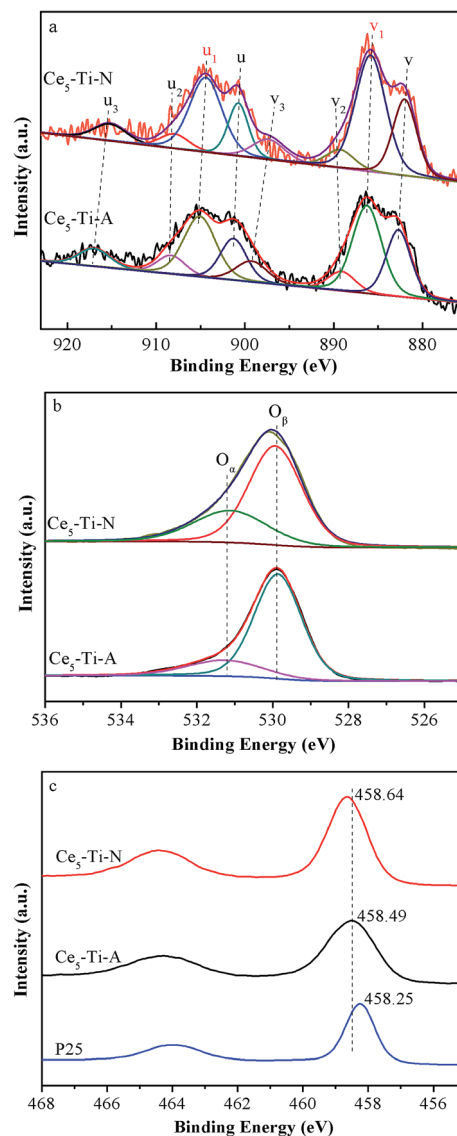

Fig. 5 XPS spectra of Ce 3d (a), O 1s (b) and Ti 2p (c) for Ce_5–Ti–A and Ce_5–Ti–N.

Ti–A, a shift to high binding energy was observed in Ce_5–Ti–N catalysts. Therefore, it suggested that more Ce–O–Ti species formed in Ce–Ti–N to decrease further density of electron cloud of Ti species. The XPS results of Ce 3d are showed in Fig. 5b and Table 2. The bands labeled as u_1 and v_1 represent the $3d^{10}4f^1$ states, ascribing to Ce^{3+}, and the other peaks represent the $3d^{10}4f^0$ states of Ce^{4+}.[25] It can be seen from Table 2 that the content of CeO_2 of Ce_5–Ti–N was higher that of Ce_5–Ti–A. This result also confirmed that the Ce species well incorporated into

Fig. 4 Raman spectra of Ce_x–Ti–A and Ce_x–Ti–N catalysts.

Table 2 The fitting data of XPS over Ce_5–Ti–A and Ce_5–Ti–N

Sample	$S_{Ce^{3+}}/(S_{Ce^{3+}} + S_{Ce^{4+}})$	$S_{O_\alpha}/(S_{O_\alpha} + S_{O_\beta})$	Ce (wt%)
Ce_5–Ti–A	36.2	19.6	3.87
Ce_5–Ti–N	49.2	30.9	3.33

the TiO_2 lattice in Ce_5–Ti–N catalyst. In addition, the ratio of Ce^{3+} increased from 36.2% in Ce_5–Ti–A to 49.2% in Ce_5–Ti–N, which indicated that more Ce^{3+} ions were retained due to the formation of Ce–O–Ti species at nitrogen calcination atmospheres. Liu *et al.* also confirmed that the incorporation of Ce species into the TiO_2 could increase the Ce^{3+} ratio because of a strong metal-support interaction (SMSI).[16] It is well-known that Ce^{3+} ions play a critical role in the oxygen storage (Ce^{3+} + $O_2 \rightarrow Ce^{4+} + O_2^-$).[26,27] Indeed, as shown in Fig. 5c and Table 2, the fitted O 1s peaks for lattice oxygen O_β (529.0–530.0 eV), chemisorbed oxygen O_α (531.3–531.9 eV) had revealed that the $O_\alpha/(O_\alpha + O_\beta)$ molar ratio in Ce_5–Ti–N was much higher than that of Ce_5–Ti–A. Since the O_α was conductive to SCR process. Therefore, it was unsurprising given that Ce–Ti–N catalysts had much higher SCR activity than that of Ce–Ti–A catalysts.

3.7 H_2-TPR analysis

The redox properties of catalysts have been known as a key factor for NH_3-SCR of NO, especially at low temperature.[28–31] Therefore, the H_2-TPR measurement was used to study the redox difference between the Ce_x–Ti–A and Ce_x–Ti–N catalysts. The H_2-TPR profiles of Ce_x–Ti–A and Ce_x–Ti–N are shown in Fig. 6. All catalysts showed two main reduction peaks, and they could be assigned to surface Ce species (at low temperature section) and the bulk Ce species (at high temperature section), respectively.[32] The two reduction peaks of Ce_x–Ti–A were enhanced with the increase of Ce species content, indicating the redox properties of Ce_x–Ti–A were related to Ce species. For Ce–Ti catalysts, Ce sites were the active redox sites to improve NO oxidation and then enhancing SCR reaction. It was obvious that the reduction peaks area of Ce_x–Ti–N was higher than that of Ce_x–Ti–A. Hence, it could be concluded that N_2 indeed improved the interaction between Ce and Ti due to more Ce into TiO_2, which consistent with Raman and XPS results. More importantly, in comparison to Ce_x–Ti–A catalysts, the surface Ce species reduction peak of Ce_x–Ti–N became stronger and shifted to lower temperature section. It proposed that the surface Ce species over Ce_x–Ti–N samples was more active than Ce_x–Ti–A. Furthermore, compared to Ce_x–Ti–A, the reduction peak of bulk Ce species in Ce_x–Ti–N became stronger and shifted to lower temperature section, indicating that the bulk Ce species on Ce_x–
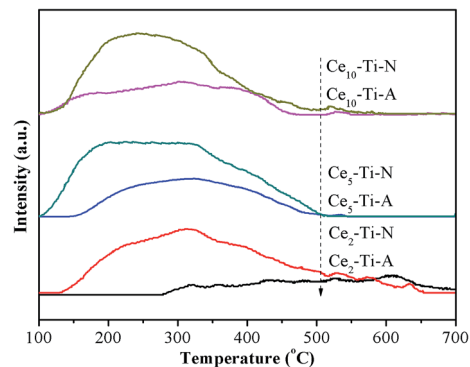
Fig. 7 NH_3-TPD results of Ce_x–Ti–A and Ce_x–Ti–N catalysts.

Ti–N could be easily reduced. These changes revealed that by N_2 treatment, the Ce_x–Ti–N catalysts had better redox properties than Ce_x–Ti–A. The better redox properties could enhance the NO oxidation that could accelerate the "fast-SCR" reaction. NO oxidation over Ce_x–Ti–N and Ce_x–Ti–A would be discussed in next section.

3.8 NH_3-TPD analysis

It is well known that the adsorption of NH_3 adsorbed on surface acid sites of SCR catalysts also plays a key role in the SCR reaction. Therefore, NH_3-TPD measurement was used for studying the total number and strength of the acid sites for Ce_x–Ti–A and Ce_x–Ti–N catalysts. The NH_3-TPD profiles of Ce_x–Ti–A and Ce_x–Ti–N are shown in Fig. 7 and Table 3. All the catalysts displayed broad NH_3-desorption patterns between 100 °C and 500 °C. The peak area of NH_3-TPD increased with the increase of Ce species content below 5% Ce content for Ce_x–Ti–A and Ce_x–Ti–N catalysts, respectively. As Ce content increased to 10%, the total acid sites decreased obviously. It could be found that the catalytic performance of Ce–Ti catalysts decreased with the increase of Ce species content. Thus, the NH_3 adsorption was not a critical role in this study. It was worth noting that the changes in the amounts of acid sites were consistent with the change in specific surface area, which proposed that the surface area played an important role in the NH_3 adsorption. However, from the Table 1, the surface area of Ce_2–Ti–N was less than that of Ce_5–Ti–A, but it showed a much higher NH_3 desorption peak in comparison with Ce_5–Ti–A. Hence, some other factors charge
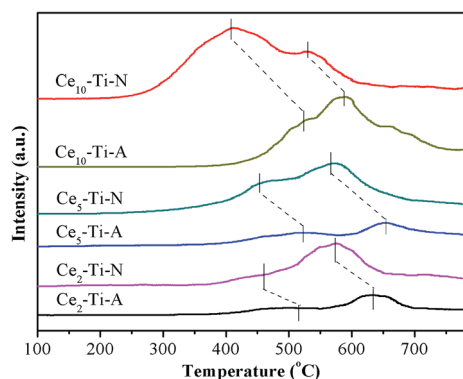
Fig. 6 H_2-TPR profiles of Ce_x–Ti–A and Ce_x–Ti–N catalysts.

Table 3   The fitting data of NH_3-TPD over Ce_x–Ti–A and Ce_x–Ti–N

Sample	Weak acid (100–250 °C) S_1/a.u.	Strong acid (>250 °C) S_2/a.u.	Total acid $S_1 + S_2$/a.u.
Ce_2–Ti–A	0	787	787
Ce_2–Ti–N	572	2124	2696
Ce_5–Ti–A	290	1054	1344
Ce_5–Ti–N	1270	1964	3234
Ce_{10}–Ti–A	410	817	1227
Ce_{10}–Ti–N	1093	1659	2752

the amounts of NH_3 adsorption. Li *et al.* confirmed that for the Ce–Ti catalyst, the Ti sites in the Ce–O–Ti short range are the acid sites for NH_3 adsorption.[12] Therefore, the difference of NH_3 adsorption between Ce_2–Ti–N and Ce_5–Ti–A might ascribe to the content of Ce–O–Ti short range. Additionally, this further confirmed that more Ce–O–Ti short range formed by calcining catalyst at the N_2 atmosphere.

3.9 *In situ* DRIFT study

In order to study the differences of NH_3 adsorption behaviors between Ce_5–Ti–A and Ce_5–Ti–N, the *in situ* DRIFT spectra of NH_3 adsorption were recorded at 240 °C. The NH_3 adsorption DRIFT spectra results of Ce_5–Ti–A and Ce_5–Ti–N are shown in Fig. 8a and b, respectively. The triplet peaks located at 3400–3100 cm^{-1} could be ascribed to the N–H stretching vibration of coordinated NH_3, the peaks located at 1850–1640 cm^{-1} and 1495–1450 cm^{-1} could be ascribed to ionic NH_4^+ on Brønsted acid sites, and the peaks located at 1610–1580 cm^{-1} and 1230–1160 cm^{-1} could be ascribed to the coordinated NH_3 on Lewis acid sites.[3,33] Notably, four band at 1598, 1353, 1222 and 1167 cm^{-1} attributed to Lewis acid sites, and a band at 1495 cm^{-1} ascribed to Brønsted acid sites could be found in the Ce_5–Ti–A spectra. For Ce_5–Ti–N, the band at 1495 cm^{-1} due to Brønsted acid sites was not detected, whereas series band located at 1840–1644 cm^{-1} because of Brønsted acid sites appearing. Hence, compared to Ce_5–Ti–A, the higher NH_3 desorption peak could attributed to emergency of new Brønsted acid sites. And these changes might attribute to the formation of a large number of Ce–O–Ti short range structures.

In situ DRIFT spectra of NO + O_2 adsorption were recorded at 240 °C to investigate the differences of adsorption nitrogen oxide species between Ce_5–Ti–A and Ce_5–Ti–N, the DRIFT spectra of NO + O_2 adsorption were recorded at 240 °C. The DRIFT spectra of NO + O_2 on Ce_5–Ti are showed in Fig. 9a. According to previous researches,[3,33,34] several peaks at 1595, 1562, 1353 and 1163 cm^{-1} could be assigned to bridging bidentate nitrates (1595 and 1163 cm^{-1}), chelating bidentate nitrates (1562 cm^{-1}) and monodentate nitrates (NO_3^-) (1353 cm^{-1}), respectively. However, as shown in Fig. 9b, eight peaks located at 1900–1600, 1540, 1380 and 1147 cm^{-1} could be observed in the DRIFT spectra of NO + O_2 on Ce_5–Ti–N. The peaks located at 1850 and 1733 cm^{-1} could be attributed to –NO^+ adsorbed on cation sites, the peaks located at 1785 and 1380 cm^{-1} could be determined as monodentate nitrates (NO_3^-), the peaks at 1676, 1622 and 1147 cm^{-1} could be ascribed to bridging bidentate nitrates, and the peaks at 1540 cm^{-1} could be assigned to chelating bidentate nitrates.[34,35] Therefore, compared with Ce_5–Ti–A, more nitrates (especially monodentate nitrates) adsorbed on the Ce_5–Ti–N sample, which indicated that the NO could be oxidized more easily over Ce_5–Ti–N than that of Ce_5–Ti–A. Previous studies suggested that redox ability of SCR catalysts resolved to NO oxidation which contributed to the "fast-SCR" route and promoted the $DeNO_x$ activity at low temperature. Combined the results of XPS and H_2-TPR in this study, the redox ability of Ce_5–Ti–N catalysts had been obviously improved due to the strong interaction between Ce and Ti by more Ce species into TiO_2. Therefore, NO oxidation was improved over Ce_5–Ti–N catalyst, thus, the Ce–Ti–N catalysts had excellent SCR activity at low temperature.
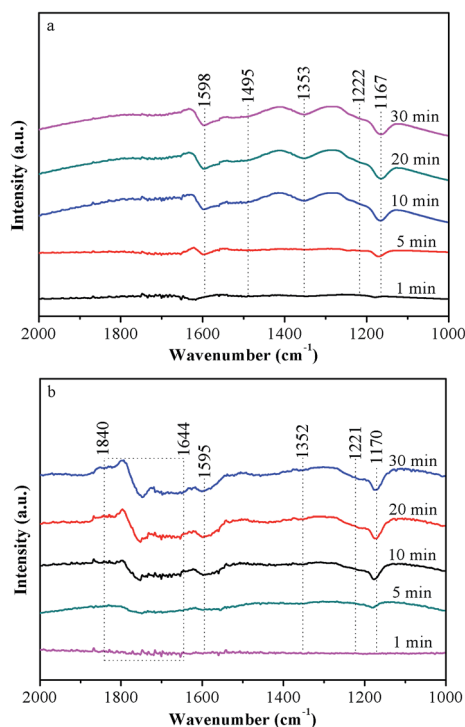

Fig. 8 *In situ* DRIFT spectra of NH_3 adsorption over Ce_5–Ti–A (a) and Ce_5–Ti–N (b) at 240 °C.
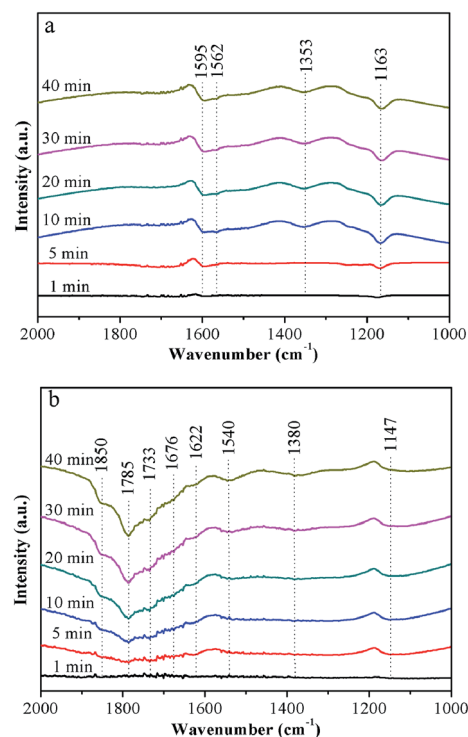
Fig. 9 *In situ* DRIFT spectra of NO + O_2 adsorption over Ce_5–Ti–A (a) and Ce_5–Ti–N (b) at 240 °C.

4.   Conclusions

In this study, we demonstrated the effect of calcination atmosphere on catalysts for NH_3-SCR reaction. The results revealed that the superior catalytic activity of Ce_x–Ti–N could be attributed to the enhancement of Ce–O–Ti short range species. The nitrogen calcination atmosphere facilitated the incorporation of Ce species into the TiO_2 lattice, hence more Ce–O–Ti short range species formed. Simultaneously, more Ce^{3+} ions retained due to incorporation of Ce species into the TiO_2 support, which could yielded enriched oxygen vacancies on catalyst surface incorporation of elements into the support for the catalysts, hence improving their catalytic activity at low temperature.

Acknowledgements

References

1 H. Bosch and F. Janssen, *Catal. Today*, 1988, **2**, 369–379.
2 G. Busca, L. Lietti, G. Ramis and F. Berti, *Appl. Catal., B*, 1998, **18**, 1–36.
3 L. A. Chen, J. H. Li and M. F. Ge, *Environ. Sci. Technol.*, 2010, **44**, 9590–9596.
4 X. Gao, Y. Jiang, Y. Zhong, Z. Y. Luo and K. F. Cen, *J. Hazard. Mater.*, 2010, **174**, 734–739.
5 Z. M. Liu, Y. Yi, J. H. Li, S. I. Woo, B. Y. Wang, X. Z. Cao and Z. X. Li, *Chem. Commun.*, 2013, **49**, 7726–7728.
6 Z. M. Liu, S. X. Zhang, J. H. Li and L. L. Ma, *Appl. Catal., B*, 2014, **144**, 90–95.
7 W. Shan, F. Liu, H. He, X. Shi and C. Zhang, *ChemCatChem*, 2011, **3**, 1286–1289.
8 W. Q. Xu, Y. B. Yu, C. B. Zhang and H. He, *Catal. Commun.*, 2008, **9**, 1453–1457.
9 S. Watanabe, X. Ma and C. Song, *J. Phys. Chem. C*, 2009, **113**, 14249–14257.
10 Z. Liu, Y. Liu, B. Chen, T. Zhu and L. Ma, *Catal. Sci. Technol.*, 2016, **6**, 6688–6696.
11 P. Li, Y. Xin, Q. Li, Z. P. Wang, Z. L. Zhang and L. R. Zheng, *Environ. Sci. Technol.*, 2012, **46**, 9600–9605.
12 Q. Li, H. C. Gu, P. Li, Y. H. Zhou, Y. Liu, Z. N. Qi, Y. Xin and Z. L. Zhang, *Chin. J. Catal.*, 2014, **35**, 1289–1298.
13 J. Ding, Q. Zhong and S. Zhang, *Ind. Eng. Chem. Res.*, 2015, **54**, 2012–2022.
14 T. Boningari, P. R. Ettireddy, A. Somogyvari, Y. Liu, A. Vorontsov, C. A. McDonald and P. G. Smirniotis, *J. Catal.*, 2015, **325**, 145–155.
15 J. Fang, X. Bi, D. Si, Z. Jiang and W. Huang, *Appl. Surf. Sci.*, 2007, **253**, 8952–8961.
16 Y. Liu, W. Y. Yao, X. L. Cao, X. L. Weng, Y. Wang, H. Q. Wang and Z. B. Wu, *Appl. Catal., B*, 2014, **160**, 684–691.
17 W. P. Shan, F. D. Liu, H. He, X. Y. Shi and C. B. Zhang, *Appl. Catal., B*, 2012, **115**, 100–106.
18 Z. M. Liu, J. Z. Zhu, J. H. Li, L. L. Ma and S. I. Woo, *ACS Appl. Mater. Interfaces*, 2014, **6**, 14500–14508.
19 K. A. Michalow-Mauke, Y. Lu, K. Kowalski, T. Graule, M. Nachtegaal, O. Krocher and D. Ferri, *ACS Catal.*, 2015, **5**, 5657–5672.
20 L. Zhang, L. L. Li, Y. Cao, X. J. Yao, C. Y. Ge, F. Gao, Y. Deng, C. J. Tang and L. Dong, *Appl. Catal., B*, 2015, **165**, 589–598.
21 W. F. Zhang, Y. L. He, M. S. Zhang, Z. Yin and Q. Chen, *J. Phys. D: Appl. Phys.*, 2000, **33**, 912.
22 G. Vlaic, R. D. Monte, P. Fornasiero, E. Fonda, J. Kašpar and M. Graziani, *J. Catal.*, 1999, **182**, 378–389.
23 F. M. Gao, D. C. Li and S. Y. Zhang, *Acta Metall. Sin.*, 2001, **37**, 445–448.
24 G. Faming and Z. Siyuan, *Rare Met.*, 2002, **21**, 299–303.
25 D. Devaiah, D. Jampaiah, P. Saikia and B. M. Reddy, *J. Ind. Eng. Chem.*, 2014, **20**, 444–453.
26 R. Maache, R. Brahmi, L. Pirault-Roy, S. Ojala and M. Bensitel, *Top. Catal.*, 2013, **56**, 658–661.
27 N. Kakuta, Y. Kudo, H. Rachi, H. Ohkita and T. Mizushima, *Top. Catal.*, 2007, **42–43**, 377–380.
28 W. P. Shan and H. Song, *Catal. Sci. Technol.*, 2015, **5**, 4280–4288.
29 C. C. Zhou, Y. P. Zhang, X. L. Wang, H. T. Xu, K. Q. Sun and K. Shen, *J. Colloid Interface Sci.*, 2013, **392**, 319–324.
30 X. P. Zhang, B. X. Shen, J. H. Chen, J. Cai, C. He and K. Wang, *J. Energy Inst.*, 2013, **86**, 119–124.
31 E. Tronconi, I. Nova, C. Ciardelli, D. Chatterjee and M. Weibel, *J. Catal.*, 2007, **245**, 1–10.
32 R. T. Guo, Y. Zhou, W. G. Pan, J. N. Hong, W. L. Zhen, Q. Jin, C. G. Ding and S. Y. Guo, *J. Ind. Eng. Chem.d*, 2013, **19**, 2022–2025.
33 L. Zhang, L. L. Li, Y. Cao, Y. Xiong, S. G. Wu, J. F. Sun, C. J. Tang, F. Gao and L. Dong, *Catal. Sci. Technol.*, 2015, **5**, 2188–2196.
34 J. B. Yu, Z. Jiang, L. Zhu, Z. P. Hao and Z. P. Xu, *J. Phys. Chem. B*, 2006, **110**, 4291–4300.
35 L. D. Li, F. X. Zhang, N. J. Guan, M. Richter and R. Fricke, *Catal. Commun.*, 2007, **8**, 583–588.